Estimation of oceanic sub-surface mixing under a severe cyclonic storm using a coupled atmosphere-ocean-wave model

Kumar Ravi Prakash, Tanuja Nigam, Vimlesh Pant

Centre for Atmospheric Sciences, Indian Institute of Technology Delhi, New Delhi-110016

Abstract

A coupled atmosphere-ocean-wave model used to examine mixing in the upper oceanic layers under the influence of a very severe cyclonic storm Phailin over the Bay of Bengal (BoB) during 10-14 October 2013. The coupled model found to improve the sea surface temperature over the uncoupled model. Model simulations highlight prominent role of cyclone induced near-inertial oscillations in sub-surface mixing up to the thermocline depth. The inertial mixing introduced by the cyclone played a central role in deepening of the thermocline and mixed layer depth by 40 m and 15 m, respectively. For the first time over the BoB, a detailed analysis of inertial oscillation kinetic energy generation, propagation, and dissipation was carried out using an atmosphere-ocean-wave coupled model during a cyclone. A quantitative estimate of kinetic energy in the oceanic water column, its propagation and dissipation mechanisms were explained using the coupled atmosphere-ocean-wave model. The large shear generated by the inertial oscillations found to overcome the stratification and initiate mixing at the base of the mixed layer. Greater mixing was found at the depths where the eddy kinetic diffusivity was large. The baroclinic current, holding a larger fraction of kinetic energy than the barotropic current, weakened rapidly after the passage of the cyclone. The shear-induced by inertial oscillations found to decrease rapidly with increasing depth below the thermocline. The dampening of mixing process below the thermocline explained through the enhanced dissipation rate of turbulent kinetic energy upon approaching the thermocline layer. The wave-current interaction, non-linear wave-wave interaction were found to affect the process of downward mixing and cause the dissipation of inertial oscillations.

1. Introduction

The Bay of Bengal (BoB), a semi-enclosed basin in the northeastern Indian ocean, consists of surplus near-surface fresh water due to large precipitation and runoff from the major river systems of the Indian subcontinent (Varkey et al., 1996; Rao and Sivakumar, 2003; Pant et al., 2015). Presence of fresh water leads to salt-stratified upper ocean water column and formation of barrier layer (BL), a layer sandwiched between bottom of the mixed layer (ML) and top of the thermocline, in the BoB (Lukas and Lindstrom, 1991; Vinayachandran et al., 2002; Thadathil et al., 2007). The BL restricts entrainment of colder waters from thermocline region into the mixed layer thereby, maintains warmer ML and sea surface temperature (SST). The warmer SST together with higher tropical cyclone heat potential (TCHP) makes the BoB as one of the active regions for cyclogenesis (Suzana et al. 2007; Yanase et al. 2012, Vissa et al. 2013). Majority of tropical cyclones generate during the pre-monsoon (April-May) and post-monsoon (October-November) seasons (Alam et al., 2003; Longshore, 2008). The number of cyclones and their intensity is highly variable in seasonal and interannual time scales. The oceanic response to the tropical cyclone depends on the stratification of the ocean. The BL formation in the BoB is associated with the strong stratification due to the peak discharge from rivers in the post-monsoon season. The intensity of the cyclone largely depends on the degree of stratification (Neetu et al. 2012; Li et al. 2013). The coupled atmosphere-ocean model found to improve the intensity of cyclonic storm when compared to the uncoupled model over different oceanic regions (Warner et al., 2010; Zambon et al., 2014; Srinivas et al., 2016; Wu et al., 2016). Zambon et al. (2014) compared the simulations from the coupled atmosphere-ocean and uncoupled models and reported significant improvement in the intensity of storm in the coupled case as compared to the uncoupled case. The uncoupled atmospheric model produced large ocean-atmosphere enthalpy fluxes and stronger winds in the cyclone (Srinivas et al., 2016). When the atmospheric model WRF was allowed interactions with the ocean model, the SST found to be more realistic as compared to the stand-alone WRF (Warner et al., 2010; Gröger et al., 2015; Jeworek et al., 2017; Hagemann et al., 2017). Wu et al. (2016) demonstrated the advantage of using a coupled model over the uncoupled model in a better simulation of typhoon Megi's intensity.

Mixing in the water column has an important role in energy and material transference. Mixing in the ocean can be introduced by the different agents such as wind, current, tide, eddy, and cyclone. Mixing due to tropical cyclones is mostly limited to the upper ocean, but the cyclone-induced internal waves can affect the subsurface mixing. Several studies have observed that the mixing in the upper oceanic layer is introduced due to the generation of near-inertial oscillations (NIO) during the passage of tropical cyclones (Gonella, 1971; Shay et al., 1989; Johanston et al., 2016). This mixing is responsible for deepening of ML and shoaling of the thermocline (Gill, 1984). The vertical mixing caused by storm-induced NIO has a significant impact on the upper ocean variability (Price, 1981). The NIO are also found to be responsible for the decrement of SST along the cyclone track (Chang and Anthes, 1979; Leipper, 1967; Shay et al., 1992; Shay et al., 2000). This decrease in SST is caused by the entrainment of cool subsurface thermocline water in the mixed layer into the immediate overlying layer of water. This cooling of surface water is one of the reasons for the decay of cyclone (Cione and Uhlhorn, 2003). The magnitude of surface cooling differs largely depending on the degree of stratification at the rightward to the cyclone track (Jacob, 2003; Price et al., 1981).

The near-inertial process can be analyzed from the baroclinic component of currents. The vertical shear of horizontal baroclinic velocities that is interrelated to buoyancy oscillations of surface layers is utilized in various studies to have an adequate understanding of the mixing associated with high-frequency oscillations, i.e. NIO (Zhang et al., 2014). The shear generated due to NIO is an important factor for the intrusion of the cold thermocline water into the ML during near-inertial scale mixing (Price et al., 1978; Shearman, 2005; Burchard and Rippeth, 2009). The alternative upwelling and downwelling features of the temperature profile are an indication of the inertial mixing. The kinetic energy bounded with these components of current shows a rise in magnitude at the right side of cyclone track (Price et al., 1981; Sanfoard et al., 1987; Jacob, 2003). The reason for this high magnitude of kinetic energy is linked with strong wind and rotating wind vector condition of the storm. The spatial distribution of near-inertial energy is primarily controlled by the boundary effect for inertial oscillations (Chen et al., 2017). The NIO is found to decline with the decreasing depth and vanishes in the coastal regions (Schahinger, 1988; Chen et al., 2017).

The aim of this paper is to understand and quantify the near-inertial mixing due to the very severe cyclonic storm Phailin in the BoB. Phailin was developed over the BoB in the northern Indian ocean in October 2013. The landfall of Phailin occurred on 12 October 2013 around 15:30 GMT near Gopalpur district of Odisha state on the east coast of India. After the 1999 super cyclonic event of the Odisha coast, Phailin was the second strongest cyclonic event that made landfall on the east coast of India (Kumar and Nair, 2015). The low-pressure system developed in the north of the Andaman Sea on 7th October 2013, which transformed into a depression on 8th October at 12 °N, 96 °E. This depression got converted to a cyclonic disturbance on 9th October and further intensified while moved to east-central BoB and opted the maximum wind speed of 200 km h^{-1} at 03:00 GMT on 11th October. Finally, landfall occurs at 17:00 GMT 12th October. More details on the development and propagation of Phailin can be found in the literature (IMD Report, 2013; Mandal et al. 2015). The performance of the coupled atmosphere-ocean model in simulating the oceanic parameters temperature, salinity, and currents during the Phailin is discussed in Prakash and Pant (2017).

Most of the past studies on the oceanic mixing under cyclonic conditions were carried out using in-situ measurements, which are constrained by the spatial and temporal availability. To the best of our knowledge, the present study is first of its kind that utilizes a coupled atmosphere-ocean-wave model over the BoB to estimate the cyclone-induced mixing and associated energy propagation at the cyclone track and a location of maximum surface wind stress during the period of peak intensity of the cyclone. The study also focuses on analyzing the subsurface distribution of NIO with its vertical mixing potential. Further, the study quantifies the shear generated mixing and the kinetic energy of the baroclinic mode of horizontal current varying in the vertical section at a selected location during the active period of the cyclone. The dissipation rate of NIO and turbulent eddy diffusivity are quantified.

2. Data and Methodology

2.1 Model details

Numerical simulations during the period of Phailin were carried out using the coupled ocean-atmosphere-wave-sediment transport (COAWST), described in detail by Warner et al. (2010). COAWST modeling system couples the three-dimensional oceanic model ‘Regional Ocean Modeling System’ (ROMS), the atmospheric model ‘Weather Research and Forecasting’ (WRF), and the wind wave generation and propagation model ‘Simulating Waves Nearshore’ (SWAN). ROMS model used for the study is a free surface, primitive equation, sigma coordinate model. ROMS is a hydrostatic ocean model that solves finite difference approximations of the Reynolds averaged Navier-Stokes equations (Chassignet et al., 2000; Haidvogel et al., 2000, Haidvogel et al., 2008; Shchepetkin and McWilliams, 2005). The atmospheric model component in the COAWST is a non-hydrostatic, compressible model 'Advanced Research Weather Research Forecast Model' (WRF-ARW), described in Skamarock et al. (2005). It has different schemes for representation of boundary layer physics and physical parameterizations of sub-grid scale processes. In the COAWST modeling system, appropriate modifications were made in the code of atmospheric model component to provide an improved bottom roughness from the calculation of the bottom stress over the ocean (Warner et al., 2010). Further, the momentum equation is modified to improve the representation of surface waves. The modified equation needs the additional information of wave energy dissipation, propagation direction, wave height, wavelength that are obtained from wave component of the COAWST model. The spectral wave model SWAN, used in the COAWST modeling system, is designed for shallow water. The wave action balance equation is solved in the wave model for both spatial and spectral spaces (Booij et al. 1999). The SWAN model used in the COAWST system includes the wave-wind generation, wave-breaking, wave-dissipation, and nonlinear wave-current-wind interaction. The 'Model Coupling Toolkit' (MCT) used as a coupler in the COAWST modeling system to couple different model components (Larson et al., 2004; Jacob et al., 2005). The coupler utilizes a parallel-coupled approach to facilitate the transmission and transformation of various distributed parameters among component models. MCT coupler exchanges prognostic variables from one model to another model component as shown in Figure 1. The WRF model receives sea surface temperature (SST) from the ROMS model and supplies the zonal (Uwind) and meridional (Vwind) components of 10-m wind, atmospheric pressure (Patm), relative humidity (RH), cloud fraction (Cloud), precipitation (Rain), shortwave (Swrad) and longwave (Lwrad) radiation to the ROMS model. The SWAN model receives Uwind and Vwind from the WRF model and transfers significant wave height (Hwave) and mean wavelength (Lmwave) to the WRF model. A large number of variables are exchanged between ROMS and SWAN models. The ocean surface current components (Us, Vs), free surface elevations (η), and bathymetry (Bath) provided to the SWAN from ROMS model. The wave parameters, i.e. Hwave, Lmwave, peak wavelength (Lpwave), wave direction (Dwave), surface wave period (Tpsurf), bottom wave period (Tmbott), percentage wave breaking (Qb), wave energy dissipation (DISSwcap), and bottom orbit velocity (Ubot) provided from the SWAN to ROMS model through the MCT coupler. Further details on the COAWST modeling system can be found in Warner et al. (2010).

2.2 Model configuration and experiment design

The coupled model was configured over the BoB to study Phailin during the period of 00 GMT 10 October – 00 GMT 15 October 2013. The setup of COAWST modeling system used in this study included fully coupled atmosphere-ocean-wave (ROMS+WRF+SWAN) models but the sediment transport is not included. A non-hydrostatic, fully compressible atmospheric model with a terrain-following vertical coordinate system, WRF-ARW (version 3.7.1) was used in the COAWST configuration. The WRF model used with 9 km horizontal grid resolution over the domain 65 °E-105 °E, 1°N-34 °N and 30 sigma levels in the vertical. The WRF was initialized with 'National Centre for Environmental Prediction' (NCEP) 'Final Analysis' (FNL) data (NCEPFNL, 2000) at 00 GMT 10 October 2013. The lateral boundary conditions in WRF were provided at 6-hour interval from the FNL data. We used the parameterization schemes for calculating boundary layer processes, precipitation processes, and surface radiation fluxes. The Monin-Obukhov scheme of surface roughness layer parameterization (Monin and Obukhov 1954) was activated in the model. The Rapid Radiation Transfer Model (RRTM) and cloud-interactive shortwave (SW) radiation scheme from Dudhia (1989) were used. The planetary boundary layer scheme YSU-PBL, described by Noh et al. (2003), was used. At each time step, the calculated value of exchange coefficients and surface fluxes off the land or ocean surface by the atmospheric and land surface layer models (NOAH) passed to the YSU PBL. The grid-scale precipitation processes were represented by WRF single-moment (WSM) six-class moisture microphysics scheme by Hong and Lim (2006). The sub-grid scale convection and cloud detrainment were taken care by Kain (2004) cumulus scheme.

A terrain following ocean model ROMS with 40 sigma levels in the vertical used in this study. The ROMS model domain used with zonal and meridional grid resolutions of 6 km and 4 km, respectively. This high resolution in ROMS enables to resolve mesoscale eddies in the ocean. The vertical stretching parameters, i.e. θ_s and θ_b were set at 7 and 2, respectively. The northern lateral boundary in ROMS was closed by the Indian subcontinent. The ROMS model observed open lateral boundaries in the west, east, and south in the present configuration. The initial and lateral open boundary conditions were derived from the 'Estimating the Circulation and Climate of the Ocean, Phase II' (ECCO2) data (Menemenlis et al., 2005). The ocean bathymetry was provided by the 2-minute gridded global relief (ETOPO2) data (National Geophysical Data Center, 2006). There was no relaxation provided to the model for any correction in the temperature, salinity, and current fields. The Generic-Length-Scale (GLS) vertical mixing scheme parameterized as the K-ε model used (Warner et al., 2005). Tidal boundary conditions were derived from the TPXO.7.2 (ftp://ftp.oce.orst.edu/dist/tides/Global) data, which includes phase and amplitude of the M2, S2, N2, K2, K1, O1, P1, MF, MM, M4, MS4, and MN4 tidal constituents along the east coast of India. The tidal input was interpolated from TPXO.7.2 grid to ROMS computational grid. The Shchepetkin boundary condition (Shchepetkin, 2005) for the barotropic current was used at open lateral boundaries of the domain which allowed the free propagation of astronomical tide and wind-generated currents. The domains of atmosphere and ocean models are shown in Figure 2. The ROMS and SWAN were configured over the common model domain shown with the shaded bathymetry data in Figure 2. The two locations used for the time series analysis are marked with stars in Figure 2. These two locations, one on-track and another off-track, were selected in the vicinity of the region of maximum surface cooling and wind-stress during the passage of Phailin. The wave model SWAN was forced with the WRF computed wind field. We used 24 frequency (0.04 - 1.0 Hz) and 36 directional bands in SWAN model. The boundary conditions for SWAN were derived from the 'WaveWatch III' model. In the COAWST system, the free surface elevations (ELV) and current (CUR) simulated by ocean model ROMS are provided to the wave model SWAN. The Kirby and Chen (1998) formulation was used for the computation of currents. The surface wind applied to the SWAN model (provided by WRF) used in the Komen et al. (1984) closure model to transfer energy from the wind to the wave field. The baroclinic time step used in ROMS model was 5 s. The SWAN and WRF models used with time steps of 120 s and 60 s, respectively. The coupled modeling system allows the exchange of prognostic variables among the atmosphere, ocean, and wave models at every 600 s. The SST simulation at high spatial and temporal resolutions enables accurate heat fluxes at the air-sea interface and exchange of heat between the oceanic mixed layer and atmospheric boundary layer. The surface roughness parameter calculated in the WRF model based on Taylor and Yelland (2001), which involved parameters from the wave model.

2.3. Methodology

The baroclinic current component was calculated by subtracting the barotropic component from the mean current with a resolution of 2 m in the vertical. The power spectrum analysis was performed on the zonal and meridional baroclinic currents along the depth section of the selected locations by using periodogram method (Auger and Flandrin, 1995). The continuous wavelet transform using Morlet wavelet method (Lilly and Olhede, 2012) carried out to analyze the temporal variability of the baroclinic current at a particular level of 14 m. The near-inertial baroclinic velocities were filtered by the Butterworth 2nd order scheme for the cutoff frequency range of 0.028 to 0.038 cycle hr^{-1}. The filtered zonal (u_f) and meridional (v_f) inertial baroclinic currents were used to calculate the inertial baroclinic kinetic energy (E_f) in m^2 s^{-2} and inertial shear (S_f) following Zhang et al. (2014) using equation (1).

$$S_f^2 = (\frac{\partial u_f}{\partial z})^2 + (\frac{\partial v_f}{\partial z})^2 \qquad (1)$$

As the stratification is a measure of oceanic stability, the buoyancy frequency (N) was calculated using equation (2)

$$N^2 = -\frac{g}{\rho}\frac{\partial \rho}{\partial z} \qquad (2)$$

Where ρ is the density of seawater and g is the acceleration due to gravity.

The analysis of generation of the inertial oscillations and their dissipation was performed on the basis of turbulent dissipation rate (ϵ) and turbulent eddy diffusivity (k_ρ).These parameters were calculated by using following formula (Mackinnon and Gregg, 2005; van der Lee and Umlauf, 2011; Palmer et al., 2008; Osborn, 1980)

$$\varepsilon = \varepsilon_0 \left(\frac{N}{N_0}\right)\left(\frac{S_{lf}}{S_0}\right) \qquad (3)$$

$$k_\rho = 0.2\, x \left(\frac{\varepsilon}{N^2}\right) \qquad (4)$$

Where S_{lf} is the low shear background velocity, Values of $N_0 = S_0 = 3$ cycle per hour and $\varepsilon_0 = 10^{-8}$ W kg^{-1}.

3. Results and Discussion

3.1. Validation of coupled model simulations

The WRF model simulated track of Phailin was validated against the India Meteorological Department (IMD) reported best-track of the cyclone. A comparison of the model-simulated track with the IMD track is shown in Figure 3. Solid circles marked on both the tracks represent the 3-

hourly positions of the cyclone's center, as identified by the minimum surface pressure. The daily positions of the centre of Phailin are labelled with the date. WRF model in the coupled configuration does a fairly good job in simulating the track, translational speed, and landfall location of Phailin. The positional track error was about 40 km when compared to IMD track of Phailin. The stand-alone WRF model (not shown here) was found to simulate Phailin track almost similar to the WRF in the coupled configuration. However, the intensity (surface wind speed) in WRF stand-alone model was higher as compared to the coupled model. Figure 4 shows the comparison of stand-alone and coupled WRF model simulated mean sea level pressure (MSLP), wind speed, and wind direction at a buoy (BD09) location (marked with a blue circle in Figure 3). It can be inferred from the figure that stand-alone WRF simulated a larger pressure drop and higher wind speed as compared to buoy measurements. In addition to the cyclone-induced pressure drop during 10-12 October, the semidiurnal variations in MSLP were observed in the buoy measurements. These semidiurnal variations in MSLP, primarily due to the radiational forcing (Pugh, 1987), were not captured by the model over the cyclone-influenced region. The WRF in coupled model configuration shows better performance in simulating the surface wind speed and pressure during Phailin. The exchange of wave parameters with the WRF model in coupled configuration provides realistic sea surface roughness that resulted in improvement of surface wind speed.

The SST simulated by the ROMS model in coupled and stand-alone configurations was validated against the Advanced Very High Resolution Radiometer (AVHRR) satellite data on each day for the period of Phailin passage over the BoB. The stand-alone WRF simulated parameters were used to provide surface boundary conditions in the stand-alone ROMS model. Figure 5 shows that the coupled model captures the SST spatial pattern reasonably well with about -0.5ºC bias in northwestern BoB on 13-14 October. This order of bias in SST could be resulted from the errors in initial and boundary conditions provided to the model. The maximum cooling of the sea surface observed on 13th October in the northwestern BoB in both, coupled model and observations. This post-cyclone cooling primarily associated with the cyclone-induced upwelling resulting from the surface divergence driven by the Ekman transport. Thus, the coupled model is reproducing dynamical processes and vertical velocities reasonably well. The stand-alone ROMS model overestimates the cyclone-induced cooling with -2.2 ºC bias in SST on 13-14 October (Figure 5).

The stronger surface winds in stand-alone WRF cause the larger cold bias in stand-alone ROMS model.

3.2. Cyclone-induced mixing

The coupled atmosphere-ocean-wave simulation is an ideal tool to understand air-sea exchange of fluxes and their effects on the oceanic water column. Surface wind sets up currents on the surface as well as initiate mixing in the interior of the upper ocean. In order to examine the strength of mixing due to Phailin, the model simulated vertical temperature profile together with the surface wind speed, zonal and meridional components of current, and kinetic energy at the on-track and off-track locations are plotted in Figure 6. Comparatively stronger zonal and meridional currents observed at the off-track location than the on-track location on 12 October. The larger kinetic energy available at the off-track location leads to greater mixing resulting into a deeper mixed layer on 12 October as compared to the on-track location. The surface wind speed at the on-track location shows a typical temporal variation of a passing cyclone. The wind speed peaks, drops, and attains second peak as the cyclone approaches, crosses over, and depart the location. The surface currents forced by these large variations in wind speed and direction at the on-track location results into comparatively weaker magnitude than the off-shore location.

The thermocline, defined as the depth of maximum temperature gradient, is usually referred to a location dependent isotherm depth (Kessler, 1990; Wang et al., 2000). Over the BoB region, the depth of 23ºC isotherm (D23) found to be an appropriate representative depth of the thermocline (Girishkumar et al., 2013). Based on the density criteria, we calculated the oceanic mixed layer depth (MLD) as the depth where density increased by 0.125 kg m^{-3} from its surface value. The inertial mixing introduced by the cyclone play central role in deepening of D23 and MLD on 12th October 2013. The warmer near-surface waters mixed downward when the cyclone crossed over this location. After the passage of cyclone, shoaling of D23 and MLD observed as a consequence of cyclone induced upwelling that entrain colder waters from the thermocline into the mixed layer. The temperature of the upper surface water (25 -30 m) decreased by 3.5°C from its maximum value of 28 °C after the landfall of the cyclone on 12-13th October at the off-shore location (Figure 6g). In response to the strong cyclonic winds, the D23 deepening by 40 m (from 50 m to 90 m) was observed during 04-12 GMT on 12 October. At the same time, the MLD, denoted by a thick black line in Figure 6g, deepens by about 15 m. On the other hand, the on-track location showed cooling at the surface only for a short time on 13 October and the deepening of D23 and MLD were 20 m and 10 m, respectively. To examine the role of cyclone induced mixing in modulating the thermohaline structure of upper ocean, we carried out further analysis on the coupled model simulations as discussed in the following sections.

3.2.1. Kinetic energy distribution

During the initial phase of Phailin, the zonal and meridional currents were primarily westward and southward, respectively (Figures 6c, 6d, 6h, and 6i). However, on and after 12th October when cyclone attains peak intensity and crosses over the location, alternative temporal sequences of westward/eastward in zonal current and southward/northward in meridional current were noticed in current profiles (Figure 6). The frequency of these reversals in zonal and meridional currents are recognized as near-inertial frequency generated from the storm at these locations. The direction and magnitude of currents represent a variability that corresponds to the presence of near-inertial oscillations at the selected locations. The kinetic energy (KE) of currents at various depths is a proxy of energy available in the water column that becomes conducive to turbulent and inertial mixing. Time series of KE associated with the barotropic and depth-averaged baroclinic components of current at the two point locations are illustrated in Figure 6e (on-track) and 6j (off-track). The KE associated with the baroclinic component found to be much higher than the barotropic component of current at both on-track and off-shore locations. The depth-averaged baroclinic and barotropic current components' KE also depict the impinging oscillatory behavior. The peak magnitude of KE in baroclinic and barotropic currents at the off-shore location found to be 1.2 $m^2\ s^{-2}$ and $0.3\times10^{-2}\ m^2\ s^{-2}$, respectively on 12th October at 08:00 GMT. Whereas the magnitude of KE in baroclinic and barotropic currents at the on-shore location was smaller than the off-shore location during the peak intensity of cyclone. The peak magnitude of kinetic energy in baroclinic current at the off-track location was more than double to that of on-track location. The comparatively smaller magnitude of KE at the on-shore location could be associated with the rapid variations in wind speed and direction leading to the complex interaction between subsurface currents in the central region of the cyclone. It is worth noting that the time of peak KE in baroclinic currents coincide with the deepening of MLD and D23. Therefore, the KE generated in NIO is responsible for sub-surface mixing that acts to deepen the mixed layer. The analysis suggests that energy available for mixing process in the water column was mostly confined to the baroclinic currents at various depths.

3.2.2. Primary frequency and depth of mixing

The power spectrum analysis was performed on the time series profiles at the two selected locations - to get a distribution of all frequencies operating in the mixing process during the passage of Phailin. The power spectrum analysis performed on the zonal and meridional components of the baroclinic current profile and shown in the Figure 7. It is clear from the figure that the tidal (M2, the semidiurnal component of tide) and near-inertial oscillations (f) are the two dominant frequencies on the surface during the cyclone Phailin. Under the influence of cyclonic winds, the NIO signal was stronger (0.84 m2s-2) at the off-track than the on-track location. The depth penetration of NIO was up to 50 m and 35 m at the off-track and on-track location, respectively. The tidal frequency (M2) and inertial frequency (f) bands shown in the Figure 7 implies that the inertial oscillations were dominant over the tidal constituent in zonal and meridional baroclinic currents. At the off-track location, the largest power of the NIO was noticed at 14 m depth, but the tidal oscillations were almost absent in the vertical section of baroclinic current (Figure 7). This finding motivated us to analyze the significance and distribution of this sub-surface variability that resulted in an anomalous deepening of MLD. The highest power of this signal at the off-track location was associated within 0-15 m with the magnitude of 0.84 m^2 s^{-1} in zonal baroclinic current and within 0-38 m with the magnitude of 0.76 m^2 s^{-1} in the meridional baroclinic current. These signals, however, weaken with increasing depth and almost disappeared around 120 m depth. These NIO were the strongest signals at the 14 m depth in the presence of local wind stress that dominated the mixing compared to any other process. Other processes include the background flows, the presence of eddies, variations in sea surface height, non-linear wave-wave and wave-current interactions (Guan et al., 2014; Park and Watts, 2005).

The second order butterworth filter was applied to the baroclinic current components to get the strength of NIO in the frequency range of 0.028 to 0.038 cycles h^{-1} at the selected locations. The filtered baroclinic current was further utilized to calculate the filtered inertial baroclinic KE (E_f in m^2s^{-2}). The daily profiles of baroclinic KE were analysed at the two selected locations and shown in Figure 8. The peak baroclinic KE differs from 0.14 m^2s^{-2} at the on-track to 0.23 m^2s^{-2} at the off-track location on 12 October. As shown in Figures 6 and 7, the filtered baroclinic KE profiles (Figure 8) confirm the dominant presence of NIO at the off-track location as compared to the on-track location. The decay of NIO with the increasing depth was noticed at both the locations. However, the NIO baroclinic KE penetrated up to 80 m in case of off-track as compared to only 50 m at the on-track location. The analysis, therefore, suggests that the NIO generated during the Phailin were more energetic at the selected off-track location, which was also the location of maximum surface cooling as noticed in Figure 5. Therefore, the further analysis in the subsequent sections is limited to the off-track location only. To analyze the time distribution of the strong NIO, wavelet transform analysis applied on the zonal and meridional baroclinic currents at 14 m depth. The Scalogram, shown in Figure 9, depicts the generation of NIO signal at the off-track location on 12th October that subsequently got strengthen and attains its peak value on the mid of 13th October. The energy percentage of the meridional component was always lower than the zonal component. The peak values of energy percentage were found in the time periods between 1-1.3 days.

3.2.3. Role of downward propagation of energy

To investigate the energy propagation from the surface to the interior layers of upper-ocean, we derived the rotary spectra (Gonella, 1972; Hayashi, 1979) of near-inertial wave numbers and shown in Figure10. The daily averaged vertical wave-number rotary spectra provides a clear picture of wind energy distribution in the sub-surface water. The anticyclonic spectrum (A_m) is dominating over the cyclonic spectra (C_m) for the entire duration of the cyclone. This feature indicates that the energy is propagating downward generated by these inertial oscillations. The magnitude of these oscillations increased from initial stage up to 12th October and remained at high energy density for the rest of the cyclone period. This downward directed energy initiated a process of mixing between the mixed layer and the thermocline. This energy helps to deepen the mixed layer against oceanic stratification by introducing a strong shear. The buoyancy of stratified ocean was overcome to some extent by the shear generated that assist in mixing process during the very severe cyclone. Alford and Gregg (2001) highlighted that in most of the cases, the energy of inertial oscillations potentially penetrates the mixed layer but suddenly drops down as it touches the thermocline. The energy dissipation mechanism studied in few other studies (Chant, 2001; Jacob, 2003).The 2-layer model described by Burchard and Rippeth (2009) illustrated the process of generation of sufficient shear to start mixing near the thermocline. Their simple model ignored the effect of the lateral density gradient, mixing, and advection. Burchard et al. (2009) mentioned four important parameters for the shear generation, i.e. surface wind stress ($P_S S^2$), bed stress ($-D_b S^2$), interfacial stress ($-D_I S^2$), and barotropic flow ($P_m S^2$). Utilizing simulations from our coupled atmosphere-ocean-wave model, we calculated individual terms as suggested by Burchard et al. (2009) and presented in Figure 10. Surface wind stress found to be the most dominating term in modulating the magnitude of bulk shear during the stormy event. Rest of the terms were relatively weaker and, therefore, contributing only marginally to the variability of the bulk shear.

To examine the generation and dissipation of these inertial oscillations, the shear generated by the near-inertial baroclinic current (S_f^2) and turbulent kinetic energy dissipation rate (ε) were calculated and analyzed. The shear produced by inertial oscillations increased at 20-80 m depth and higher magnitude was associated with peak wind speed of cyclone (Figure 12a). This shear overcome the stratification (Figure 12b), represented by buoyancy frequency N^2, and played important role in mixing and deepening of the thermocline and mixed layer on 12th October. The value of kinetic energy dissipation rate (ε) increased from 4×10^{-14} to 2.5×10^{-13} W kg^{-1} on approaching the thermocline (Figure 12c). The increase in ε indicates the weakening of the shear generated by the inertial waves leading to the fast disappearance of these baroclinic instabilities from the region. The non-linear interaction between the NIO and internal tides together with the prevailing background currents cause rapid dissipation of kinetic energy in the thermocline. Guan et al. (2014) also reported an accelerated dampening of NIO associated with the wave-wave interactions between NIO and internal tides. The background currents found to modify the propagation of NIO (Park and Watts, 2005). The magnitude of the turbulent eddy diffusivity (K_ρ), shown in Figure 12d, implies that the greater mixing takes place within the mixed layer where K_ρ was high (6.3×10^{-11} to 1.2×10^{-11} m^2 s^{-1}). The daily averaged values of ε and K_ρ were 1.2×10^{-13} W kg^{-1} and 1.5×10^{-10} m^2 s^{-1}, respectively on 12th October, which were higher as compared to the initial two days of the cyclonic event. Results from the present study, as well as the conclusions from the past studies, indicate that wave-current interaction, mesoscale processes, and wave-wave interaction can affect the process of downward mixing and cause the dissipation of inertial oscillations.

4. Conclusions

Processes controlling the sub-surface mixing were evaluated under the high wind speed regime of the severe cyclonic storm Phailin over the BoB. A coupled atmosphere-ocean-wave (WRF+ROMS+SWAN) model as part of the COAWST modeling system was used to simulate atmospheric and oceanic conditions during the passage of Phailin cyclone. A detailed analysis of model-simulated data revealed interesting features of generation, propagation, and dissipation of kinetic energy in the upper oceanic water column. Deepening of the MLD and thermocline by 15 m and 40 m, respectively were explained through the strong shear generated by the inertial oscillations that helped to overcome the stratification and initiate mixing at the base of the mixed layer. However, there was a rapid dissipation of the shear with increasing depth below the thermocline. The peak magnitude of kinetic energy in baroclinic and barotropic currents found to be 1.2 $m^2 s^{-2}$ and 0.3×10^{-2} $m^2 s^{-2}$, respectively. The power spectrum analysis suggested a dominant frequency operative in sub-surface mixing that was associated with near-inertial oscillations. The peak strength of 0.84 $m^2 s^{-1}$ in the zonal baroclinic current found at 14 m depth at a location in northwestern BoB. The baroclinic kinetic energy remained higher (> 0.03 $m^2 s^{-2}$) during 11-12 October and decreased rapidly after that. The wave-number rotary spectra identified the downward propagation, from the surface up to the thermocline, of energy generated by inertial oscillations. A quantitative analysis of shear generated by the near-inertial baroclinic current showed higher shear generation at 20-80 m depth during peak surface winds. Analysis highlights that greater mixing within the mixed layer takes place where the eddy kinetic diffusivity was high (> 6×10^{-11} $m^2 s^{-1}$). The turbulent kinetic energy dissipation rate increased from 4×10^{-14} to 2.5×10^{-13} W kg^{-1} on approaching the thermocline that dampened mixing process further down into the thermocline layer. The wave-current interaction, mesoscale processes, and wave-wave interaction increased the dissipation rate of shear and, thereby, limited the downward mixing up to the thermocline. The coupled model found to be a useful tool to investigate air-sea interaction, kinetic energy propagation, and mixing in the upper-ocean. The results from this study highlight the importance of atmosphere-ocean coupling for a better understanding of oceanic response under the strong wind conditions. The proper representation of kinetic energy propagation and oceanic mixing have applications in improving the intensity prediction of a cyclone, storm surge forecasting, and biological productivity.

Author contribution: KRP and TN performed model simulations and analyzed data. VP prepared the manuscript with contributions from all co-authors.

Acknowledgements

ECCO2 is a contribution to the NASA Modeling, Analysis, and Prediction (MAP) program. The study benefitted from the funding support from Ministry of Earth Sciences, Govt. of India and Space Applications Centre, Indian Space Research Organisation. High Performance Computing (HPC) facility provided by IIT Delhi and Department of Science and Technology (DST-FIST 2014 at CAS), Govt. of India are thankfully acknowledged. Authors are thankful to Dr. Lingling Xie for his productive suggestions. Graphics generated in this manuscript using Ferret and NCL. The constructive comments from three anonymous reviewers helped to improve the manuscript. TN and KRP acknowledge MoES and UGC-CSIR, respectively for their PhD fellowship support.

References

Alam, M. M., Hossain, M.A. and Shafee, S.: Frequency of Bay of Bengal cyclonic storms and depressions crossing different coastal zones, Int. J. Climatol., 23, 1119–1125, doi:10.1002/joc.927, 2003.

Alford, M.H., Gregg, M.C.: Near-inertial mixing: modulation of shear, strain and microstructure at low latitude. J. Geophys. Res. 106 (C8), 16947–16968, 2001.

Auger F., Flandrin, P.: Improving the Readability of Time-Frequency and Time-Scale Representations by the Reassignment Method. IEEE Transactions on Signal Processing. 43, 1068–1089, 1995.

Booij, N., Ris, R. C., and Holthuijsen, L. H.: A third-generation wave model for coastal regions, Part I, Model description and validation, J. Geophys. Res., 104(C4), 7649–7666, doi:10.1029/98JC02622, 1999.

Burchard, H., Rippeth, T.P.: Generation of bulk shear spikes in shallow stratified tidal seas. J. Phys. Oceanogr. 39, 969–985, 2009.

Chang, S. W., and Anthes, F.A.: The mutual response of the tropical cyclone and the ocean. J. Phys. Oceanogr., 9, 128–135, 1979.

Chant, R.J.: Evolution of near-inertial waves during an upwelling event on the New Jersey Inner Shelf. J. Phys. Oceanogr. 31, 746–764, 2001.

Chen, S., Chen, D., Xing, J.: A study on some basic features of inertial oscillations and near-inertial internal waves. Ocean Science, 13 (5), 829-836, 2017.

Chassignet, E.P., Arango, H.G., Dietrich, D., Ezer, T., Ghil, M., Haidvogel, D.B., Ma, C.C., Mehra, A., Paiva, A.M., Sirkes, Z.: DAMEE-NAB: the base experiments. Dyn. Atmos. Oceans 32, 155–183, 2000.

Cione, J. J., and Uhlhorn, E.W.: Sea surface temperature variability in hurricanes: Implications with respect to intensity change, Mon. Weather Rev., 131, 1783–1796, doi:10.1175//2562.1, 2003.

Dudhia, J.: Numerical study of convection observed during the winter monsoon experiment using a mesoscale two dimensional model. J Atmos Sci. 46, 3077–3107, 1989.

Gill, A. E.: On the behavior of internal waves in the wake of storms,J. Phys. Oceanogr., 14, 1129 – 1151, 1984.

Girishkumar, M. S., Ravichandran, M., Han, W.: Observed intraseasonal thermocline variability in the Bay of Bengal. J. Geophys. Res. Oceans, 118, 3336–3349, doi:10.1002/jgrc.20245, 2013.

Gonella, J.: A study of inertial oscillations in the upper layers of the oceans. Deep-Sea Res., 18, 775–788, 1971.

Gonella, J.: A rotary-component method for analysing meteorological and oceanographic vector time series. Deep-Sea Research 19, 833–846, 1972.

Gröger M, Dieterich C, Meier HEM, Schimanke S: Thermal air-sea coupling in hindcast simulations for the North Sea and Baltic Sea on the NW European shelf. Tellus A Dyn Meteorol Oceanogr 67(1):26911. doi: 10.3402/tellusa.v67.26911, 2015.

Guan, S., Zhao, W., Huthnance, J. Tian, J., and Wang, J.: Observed upper ocean response to typhoon Megi (2010) in the Northern South China Sea. J. Geophys. Res. Oceans, 119, 3134–3157, doi:10.1002/2013JC009661, 2014.

Haidvogel, D.B., Arango, H.G., Budgell, W.P., Cornuelle, B.D., Curchitser, E., Di Lorenzo, E., Fennel, K., Geyer, W.R., Hermann, A.J., Lanerolle, L., Levin, J., McWilliams, J.C., Miller, A.J., Moore, A.M., Powell, T.M., Shchepetkin, A.F., Sherwood, C.R., Signell, R.P., Warner, J.C., Wilkin, J.: Regional ocean forecasting in terrain-following coordinates: model formulation and skill assessment. Journal of Computational Physics 227, 3595–3624, 2008.

Haidvogel, D.B., Arango, H.G., Hedstrom, K., Beckmann, A., Malanotte-Rizzoli, P. Shchepetkin, A.F.: Model evaluation experiments in the North Atlantic Basin: Simulations in nonlinear terrain-following coordinates. Dyn Atmos Oceans 32, 239–281, 2000.

Hayashi, Y.: Space-time spectral analysis of rotary vector series. J. Atmos. Sci. 36 (5), 757–766, 1979.

Ho-Hagemann, H.T.M., Gröger, M., Rockel, B., Zahn, M., Geyer, B., Meier, H.E.M: Effects of air-sea coupling over the North Sea and the Baltic Sea on simulated summer precipitation over Central Europe, Clim Dyn 49, 3851. https://doi.org/10.1007/s00382-017-3546-8, 2017.

Hong, S.Y., Lim, J.O.J.: The WRF single-moment 6-class microphysics scheme (WSM6). J Korean Meteor Soc 42:2, 129-151, 2006.

IMD Report.: Very Severe Cyclonic Storm, PHAILIN over the Bay of Bengal (08-14 October 2013) A Report. India Meteorological Department, Technical Report, October 2013.

Jacob, S.D., Shay, L.K.: The role of oceanic mesoscale features on the tropical cyclone-induced mixed layer response: A case study. J. Phys. Oceanog., 33, 649- 676, 2003.

Jacob, R., Larson, J., Ong, E.: M x N Communication and Parallel Interpolation in CCSM Using the Model Coupling Toolkit. Preprint ANL/MCSP1225-0205. Mathematics and Computer Science Division, Argonne National Laboratory, 25 pp, 2005.

Jeworrek, J., Wu, L., Dieterich, C., and Rutgersson, A.: Characteristics of convective snow bands along the Swedish east coast, Earth Syst. Dynam., 8, 163-175, https://doi.org/10.5194/esd-8-163-2017, 2017.

Johnston, T.M.S., Chaudhuri, D., Mathur, M., Rudnick, D.L., Sengupta, D., Simmons, H.L., Tandon, A., and Venkatesan, R.: Decay mechanisms of near-inertial mixed layer oscillations in the Bay of Bengal, Oceanography, 29(2): 180–191, doi:10.5670/oceanog.2016.50, 2016.

Kain, J.S.: The Kain-Fritsch convective parameterization: An update. J Appl Meteor 43, 170–181, 2004.

Kessler, W. S.: Observations of long Rossby waves in the northern tropical Pacific. J. Geophys. Res., 95, 5183–5217, 1990.

Kirby, J. T., and Chen T.M.: Surface waves on vertically sheared flows Approximate dispersion relations. J. Geophys. Res., 94(C1),1013–1027, doi:10.1029/JC094iC01p01013, 1989.

Komen, G.J., Hasselmann, S., and Hasselmann, K.: On the existence of a fully developed wind-sea spectrum. J. Phys. Oceanogr., 14, 1271–1285. 1984.

Kumar VS, Nair A.M.: Inter-annual variations in wave spectral characteristics at a location off the central west coast of India. Ann Geophys 33:159–167, doi:10.5194/angeo-33-159, 2015.

Leipper, D. F.: Observed Ocean Conditions and Hurricane Hilda, 1964, J. Atmos. Sci., 24, 182–186, doi:10.1175/1520-0469(1967) 0242.0.CO;2, 1967.

Zhi, Li., Yu, W., Li, T., Murty, V.S.N., and Tangang, F.: Bimodal character of cyclone climatology in the Bay of Bengal modulated by monsoon seasonal cycle. J Climate 26:1033-1046. doi: 10.1175/JCLI-D-11-00627.1, 2013.

Lilly, J. M., Olhede, S. C.: Generalized Morse Wavelets as a Superfamily of Analytic Wavelets. IEEE Transactions on Signal Processing. 60 (11), 6036–6041, 2012.

Longshore, D.: Encyclopedia of Hurricanes, Typhoons, and Cyclones, 468 pp., Checkmark, New York, 2008.

Larson, J., Jacob, R., Ong, E.: The Model Coupling Toolkit: A New Fortran90 Toolkit for Building Multiphysics Parallel Coupled Models. Preprint ANL/MCS- P1208-1204. Mathematics and Computer Science Division, Argonne National Laboratory, 25 pp, 2004.

Lukas, R., and Lindstrom, E.: The mixed layer of the western equatorial Pacific Ocean, J. Geophys. Res., 96, 3343–3357, 1991.

MacKinnon, J.A., Gregg, M.C.: Spring Mixing: Turbulence and Internal Waves during Restratification on the New England Shelf. Journal of Physical Oceanography. 35:12, 2425-2443 2005.

Mandal M., Singh K. S., Balaji M., Mohapatra M.: Performance of WRF-ARW model in real-time prediction of Bay of Bengal cyclone 'Phailin'. Pure Appl. Geophys DOI 10.1007/s00024-015-1206-7, 2015.

Menemenlis, D., et al., NASA supercomputer improves prospects for ocean climate research, Eos Trans. AGU, 86(9), 89–96, doi:10.1029/2005EO090002, 2005.

Monin, A.S., Obukhov, A.M.F.: Basic laws of turbulent mixing in the surface layer of the atmosphere. *Contrib Geophys Inst Acad Sci USSR 151:*163, e187, 1954.

National Centers for Environmental Prediction/National Weather Service/NOAA/U.S. Department of Commerce: NCEP FNL Operational Model Global Tropospheric Analyses, continuing from July 1999. Research Data Archive at the National Center for Atmospheric Research, Computational and Information Systems Laboratory. Dataset. https://doi.org/10.5065/D6M043C6, 2000.

National Geophysical Data Center. 2-minute Gridded Global Relief Data (ETOPO2) v2. National Geophysical Data Center, NOAA. doi:10.7289/V5J1012Q, 2006.

Neetu, S., Lengaigne, M., Vincent, E.M., Vialard, J., Madec, G., Samson, G., Ramesh Kumar, M.R., and Durand, F.: Influence of upper-ocean stratification on tropical cyclone-induced surface cooling in the Bay of Bengal, J. Geophys. Res., 117, C12020, doi:10.1029/2012JC008433, 2012.

Noh, Y., Cheon, W.G., Hong, S.Y., Raasch, S.: Improvement of the K-profile model for the planetary boundary layer based on large eddy simulation data. Bound Layer Meteor 107, 401–427, 2003.

Osborn, T.R.: Estimates of the Local-Rate of Vertical Diffusion from Dissipation Measurements. J. Phys. Oceanogr. 10, 83–89, 1980.

Palmer, M.R., Rippeth, T.P., Simpson, J. H.: An investigation of internal mixing in a seasonally stratified shelf sea. J. Geophys. Res. 113, C12005, doi:10.1029/2007JC004531, 2008.

Pant V, Girishkumar M.S., Udaya Bhaskar T.V.S., Ravichandran M., Papa F., Thangaprakash V.P.: Observed interannual variability of near-surface salinity in the Bay of Bengal, J. Geophys. Res 120(5):3315–3329, 2015.

Park, J.H., and Watts, D. R.: Near-inertial oscillations interacting with mesoscale circulation in the southwestern Japan/East Sea. Geophys. Res. Lett., 32, L10611, doi: 10.1029/2005GL022936, 2005.

Prakash K.R., Vimlesh Pant: Upper oceanic response to tropical cyclone Phailin in the Bay of Bengal using a coupled atmosphere-ocean model, Ocean Dynamics, 67, 51-64, doi:10.1007/s10236-016-1020-5, 2017.

Price, J. F., Mooers, C.N., and Van Leer, J.C.: Observation and simulation of storm-induced mixed-layer deepening. J. Phys. Oceanogr., 8, 582-599, https://doi.org/10.1175/1520-0485(1978)008<0582:OASOSI>2.0.CO;2, 1978.

Price, J.F.: Upper ocean response to a hurricane. J. Phys. Oceanog., 11, 153-175, 1981.

Pugh, D.T.: Tides, Surges and Mean Sea-Level, John Wiley & Sons, Chichester, 472 pp., 1987.

Rao, R. R., and Sivakumar, R.: Seasonal variability of sea surface salinity and salt budget of the mixed layer of the north Indian Ocean, J. Geophys. Res., 108(C1), 3009, doi:10.1029/2001JC000907, 2003.

Sanford, T. B., Black, P.G., Haustein, J., Feeney, J.W., Forristall, G.Z., and Price, J.F.: Ocean response to a hurricane. Part I: Observations. J. Phys. Oceanogr., 17, 2065–2083, 1987.

Schahinger, R.B.: Near inertial motion on the south Australian shelf. J. Phys. Oceanogr., 18(3), 492-504, 1988.

Shchepetkinand A. F., McWilliams J. C.: The Regional Ocean Modeling System: A split-explicit, free-surface, topography following coordinates ocean model, *Ocean Modelling*, **9**, 347-404, 2005.

Skamarock, W.C., Klemp, J.B., Dudhia, J., Gill, D.O., Barker, D.M., Wang, W., Powers, J.G.: A Description of the Advanced Research WRF Version 2. NCAR Technical Note, NCAR/TN-468+STR., 2005.

Shay, L. K., Black, P., Mariano, A., Hawkins, J., and Elsberry, R.: Upper ocean response to hurricane Gilbert, J. Geophys. Res., 97(20), 227–248, 1992.

Shay, L. K. and Elsberry, R.L.: Vertical structure of the ocean current response to a hurricane. J. Phys. Oceanog., 19, 649-669, 1989.

Shay, L. K., Goni, G.J., and Black, P.G.: Effects of a warm oceanic feature on Hurricane Opal, Mon. Weather Rev., 128, 1366–1383, doi:10.1175/1520-0493(2000)1282.0.CO;2, 2000.

Shearman, R.K.: Observations of near-inertial current variability on the New England shelf. J. Geophys. Res. 110, C02012, doi:10.1029/2004JC002341, 2005.

Srinivas, C. V., Mohan,G. M., Naidu, C. V., Baskaran, R., Venkatraman B. :Impact of air-sea coupling on the simulation of tropical cyclones in the North Indian Ocean using a simple 3-D ocean model coupled to ARW, J. Geophys. Res. Atmos., 121, 9400,9421, doi:10.1002/2015JD024431, 2016.

Suzana, J Carmargo, Adam H Sobel, Anthony G Barnston and Kerry A. Emanuel: Tropical cyclone genesis potential index in climate models. Tellus 59A:428-443, 2007.

Taylor, P.K., Yelland, M.J.: The dependence of sea surface roughness on the height and steepness of the waves. J. Phys. Oceanogr., 31, 572–590, 2001.

Thadathil, P., Muraleedharan, P.M., Rao, R.R., Somayajulu, Y.K., Reddy, G.V., and Revichandran, C.: Observed seasonal variability of barrier layer in the Bay of Bengal, J. Geophys. Res., 112, C02009, doi:10.1029/2006JC003651, 2007.

Varkey, M. J., Murty, V.S.N., and Suryanarayana, A.: Physical oceanography of the Bay of Bengal and Andaman Sea, Oceanogr. Mar. Biol., 34, 1–70, 1996.

van der Lee, E.M., and Umlauf, L.: Internal wave mixing in the Baltic Sea: near-inertial waves in the absence of tides. J. Geophys. Res. 116, C10016, doi:10.1029/2011JC007072, 2011.

Vinayachandran, P. N., Murty, V.S.N., and Ramesh Babu V.: Observations of barrier layer formation in the Bay of Bengal during summer monsoon, J. Geophys. Res., 107(C12), 8018, doi:10.1029/2001JC000831, 2002.

Vissa, N.K., Satyanarayana, A.N.V. and Prasad Kumar, B.: Intensity of tropical cyclones during pre- and post-monsoon seasons in relation to accumulated tropical cyclone heat potential over Bay of Bengal, Nat Hazards 68: 351. https://doi.org/10.1007/s11069-013-0625-y. 2013.

Wang, B., Wu, R., and Lukas R.: Annual adjustment of the thermocline in the tropical Pacific Ocean, J. Clim., 13, 596–616, 2000.

Warner, J. C., Sherwood, C.R., Arango, H.G., and Signell, R.P.: Performance of four turbulence closure models implemented using a generic length scale method, Ocean Modell., 8, 81–113, doi:10.1016/j. ocemod.2003.12.003, 2005.

Warner, J.C., Armstrong B., He R., Zambon J.B.: Development of a coupled ocean–atmosphere–wave–sediment transport (COAWST) modeling system. Ocean modelling 35:230–244. doi:10.1016/j. oceanmod.2010.07.010, 2010.

Yanase, W., Satosh, M., Taniguchi, H., and Fujinami, H.: Seasonal and Intraseasonal Modulation of tropical cyclogenesis environment over the Bay of Bengal during the extended summer monsoon. J Climate 25:2914-2930. doi: 10.1175/JCLI-D-11-00208.1, 2012.

Zhang, S., Xie, L., Hou, Y., Zhao, H., Qi, Y., & Yi, X.: Tropical storm-induced turbulent mixing and chlorophyll-a enhancement in the continental shelf southeast of Hainan Island. *Journal of Marine Systems*, *129*, 405-414, 2014.

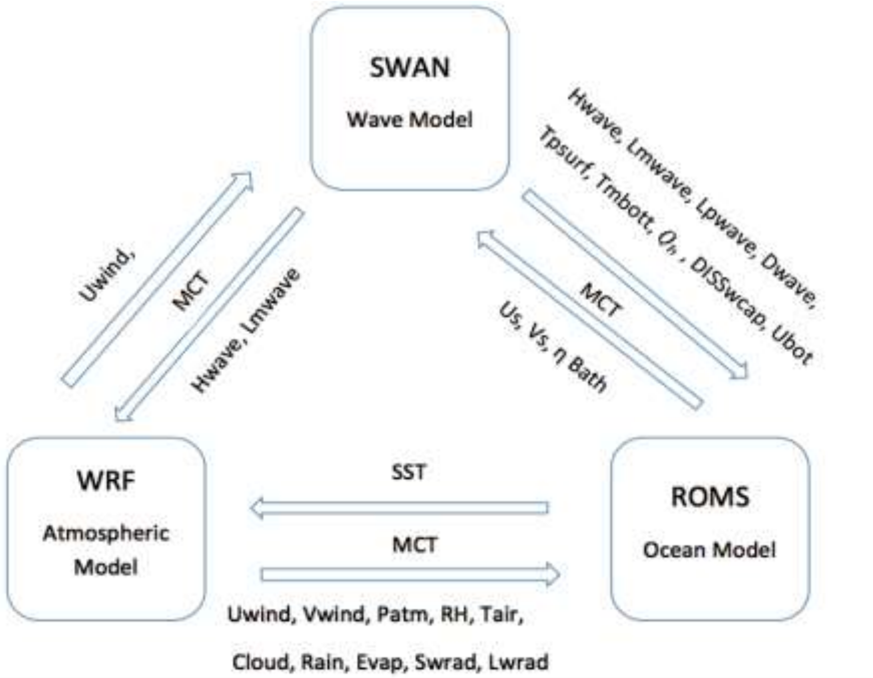

Figure 1:-The block diagram showing the component models WRF, ROMS, and SWAN of the COAWST modeling system together with the variables exchanged among the models. MCT- the model coupling toolkit is a model coupler used in the COAWST system.

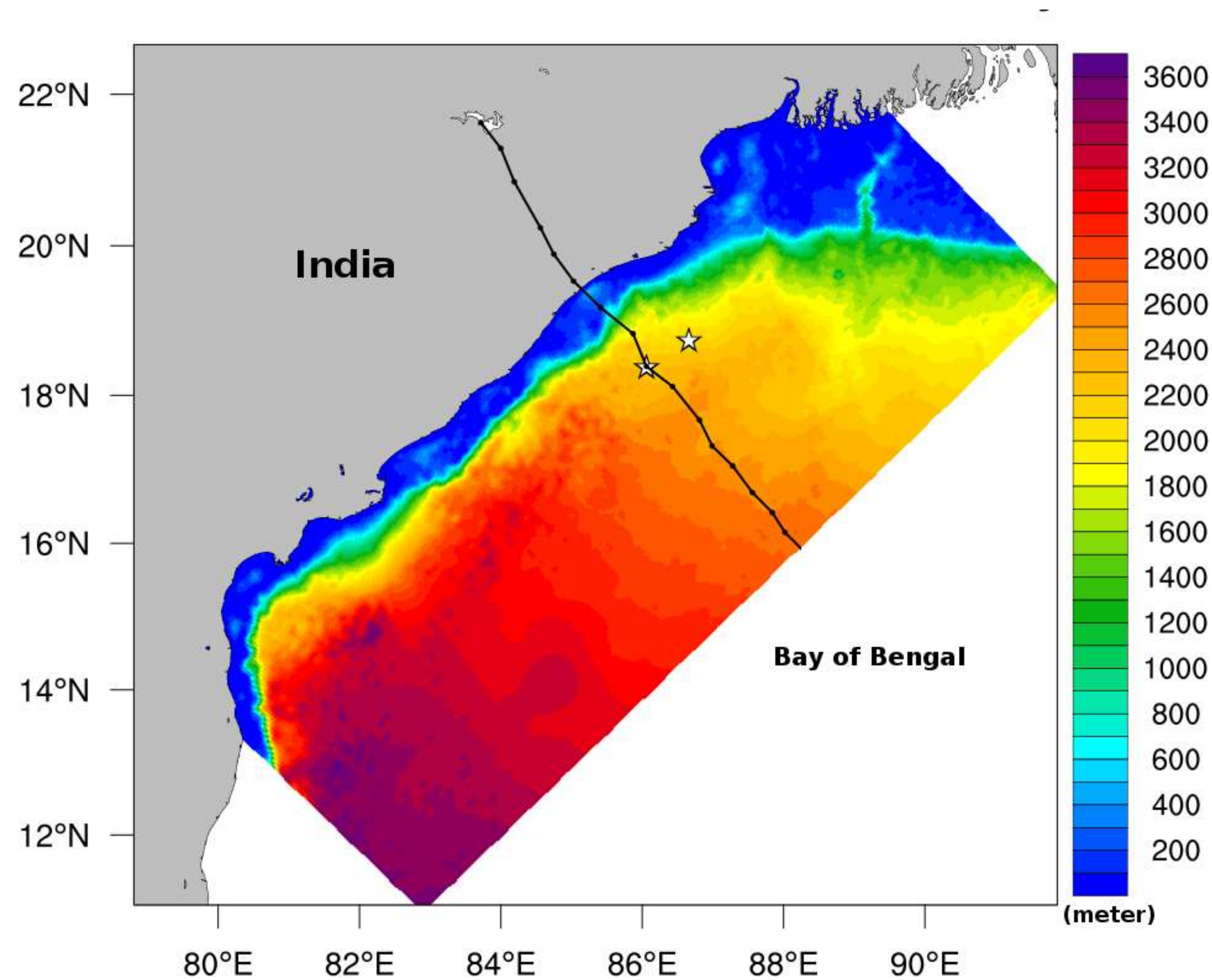

Figure 2:-COAWST model domain (65°-105 °E, 1°-34 °N) overlaid with GEBCO bathymetry (m). Locations used for time-series analysis are marked with stars.

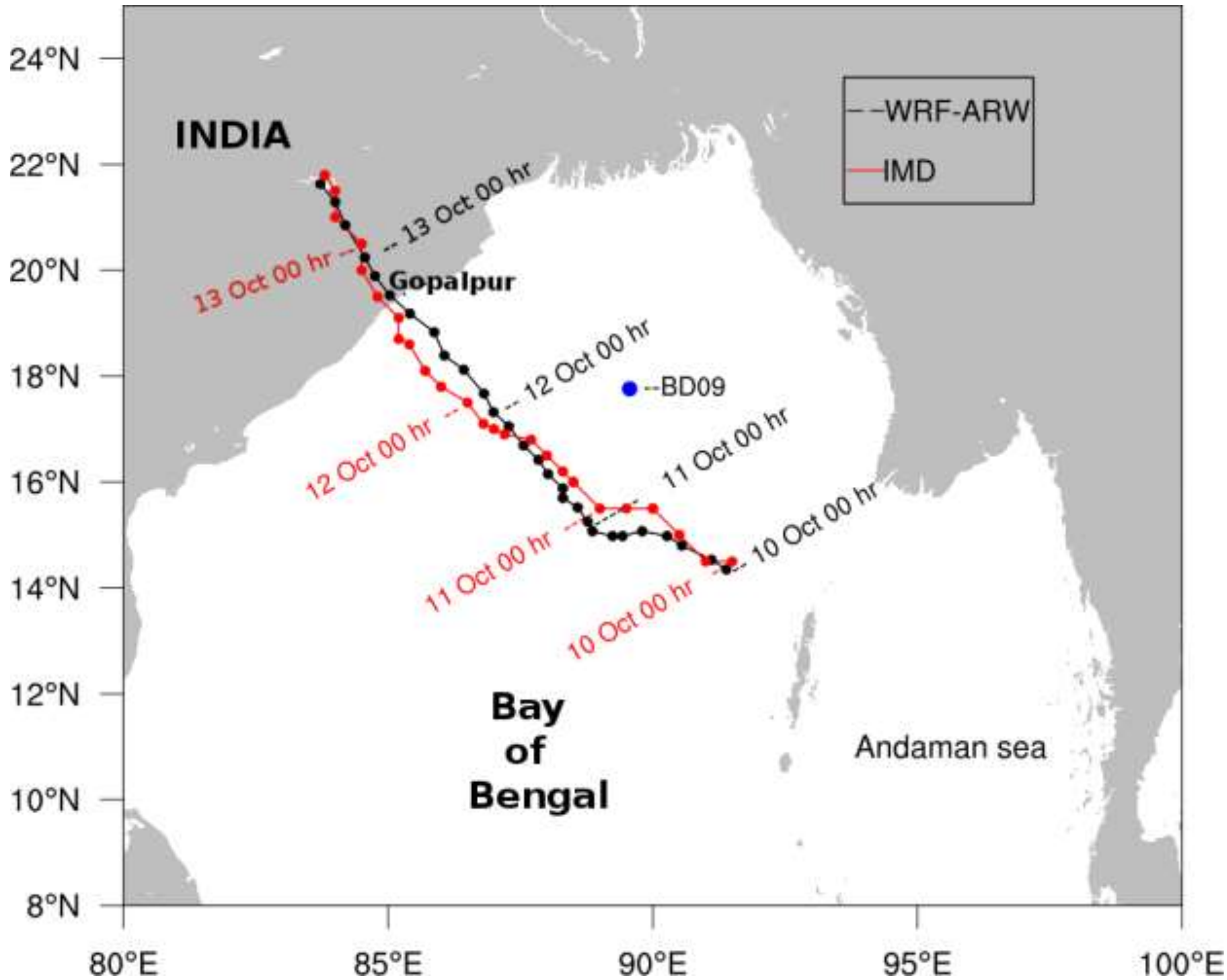

Figure 3:- Tracks of Phailin simulated by the coupled model (black) and IMD reported (red). The 3-hourly positions of the center of Phailin marked with solid circles and the daily position at 00 hr are labelled with the dates. Location of buoy BD09 is marked with a blue circle.

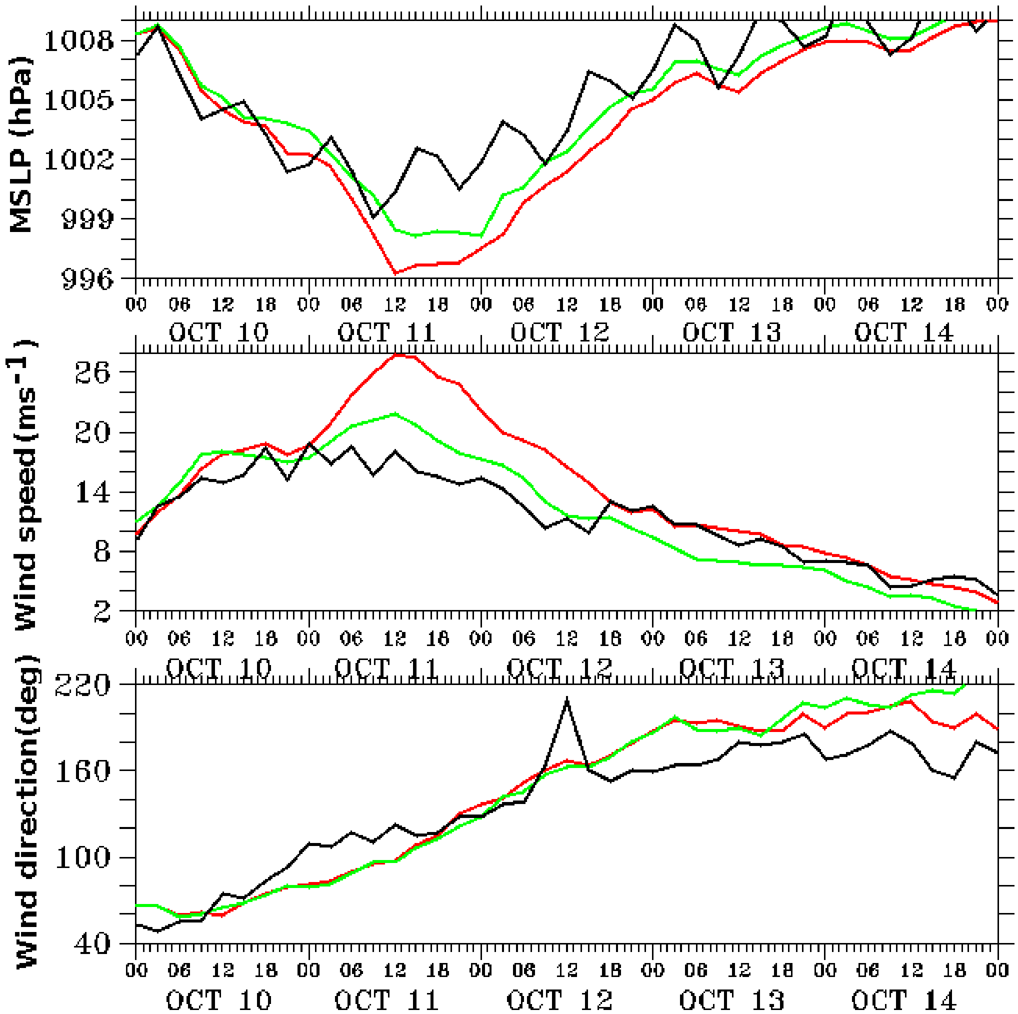

Figure 4: Comparison of coupled model (green), stand-alone WRF model (red), and observations from a buoy BD09 (black) for the (top panel) mean sea level pressure (hPa), (middle panel) wind speed (ms^{-1}), and (bottom panel) wind direction (degree).

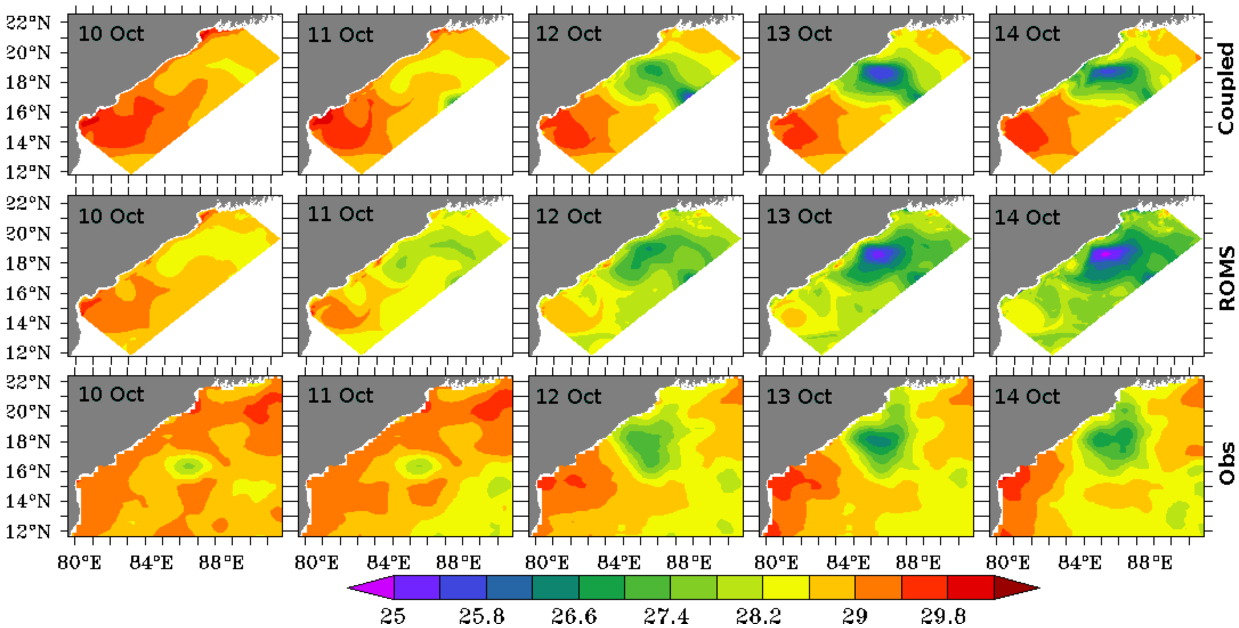

Figure 5:- The daily averaged sea surface temperature (SST) in °C simulated by the coupled model (upper panel), stand alone ROMS model (middle panel), and observed from AVHRR sensor on the satellite (lower panel)..

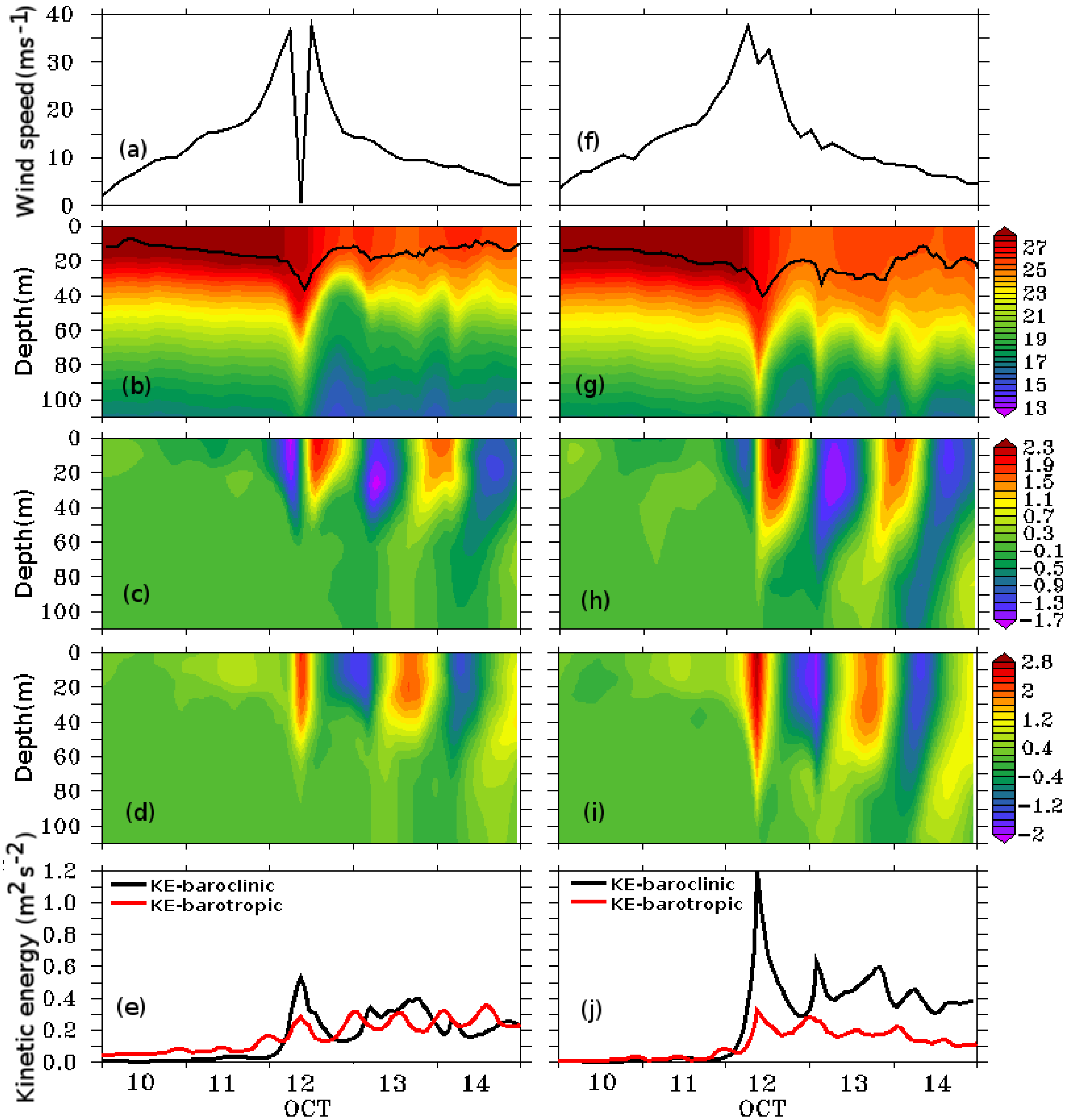

Figure 6: Coupled model simulated and diagnosed variables at the on-track (left panel) and off-track (right panel) locations. (a, f) Surface wind speed (ms^{-1}), (b, g) temperature profile (°C) and mixed layer depth (black line), (c, h) u-component of current (ms^{-1}), (d, i) v-componenet of current (ms^{-1}), (e, j) Kinetic energy of baroclinic (m^2s^{-2}) and barotropic ($\times 10^{-2}$ m^2s^{-2}) current.

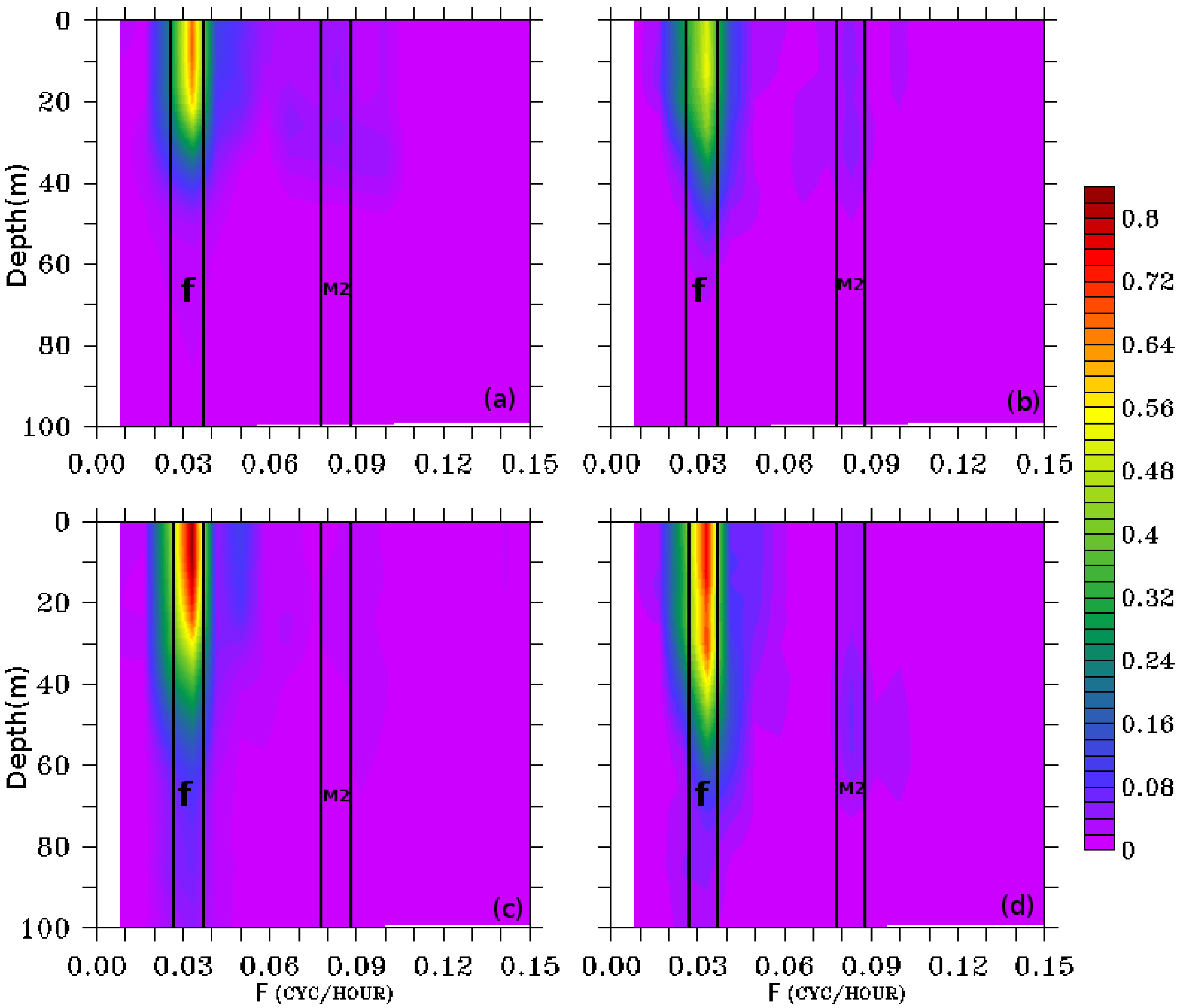

Figure 7:- The power spectrum analysis (m^{2}s^{-1}) performed on the simulation period at the on-track (upper panel) and off-track (lower panel) locations for (a, c) baroclinic zonal current and (b, d) baroclinic meridional current.

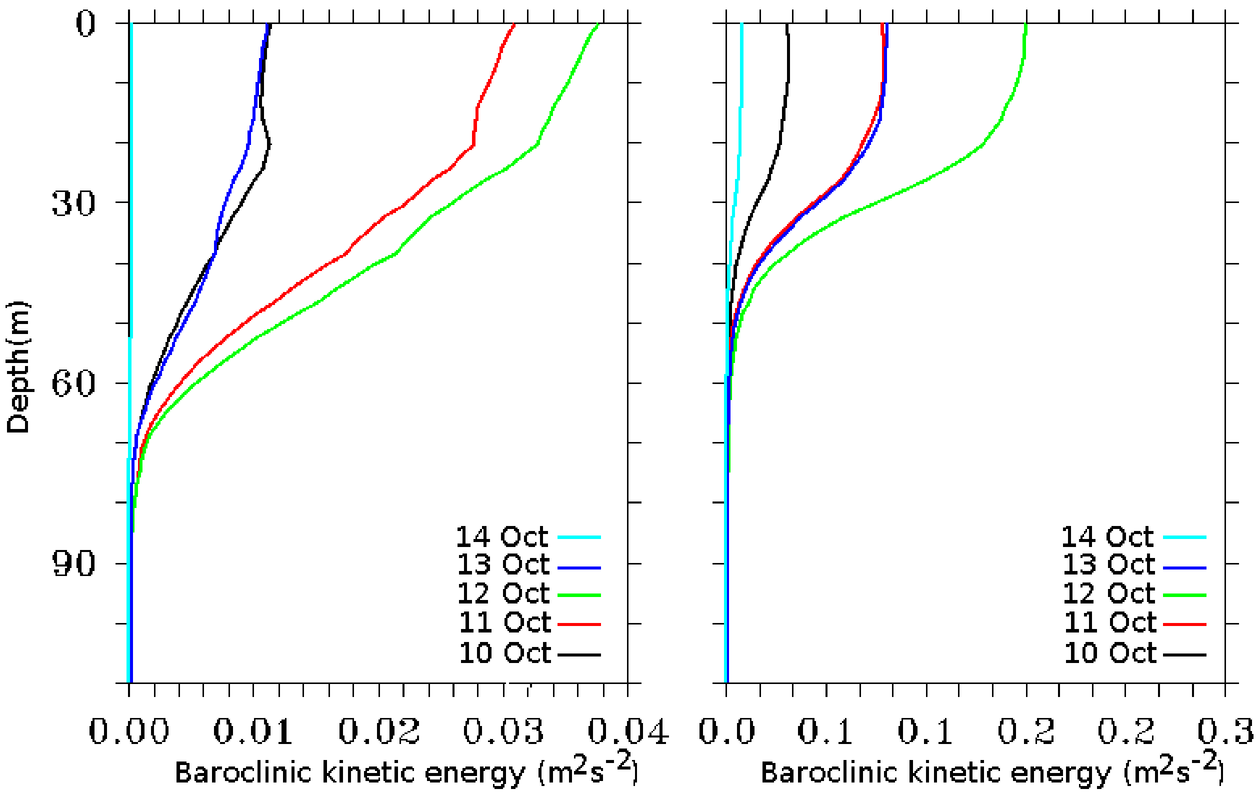

Figure 8: Daily averaged baroclinic kinetic energy (m^2s^{-2}) profile at the on-track (left) and off-track (right) locations as marked with stars in Figure 2.

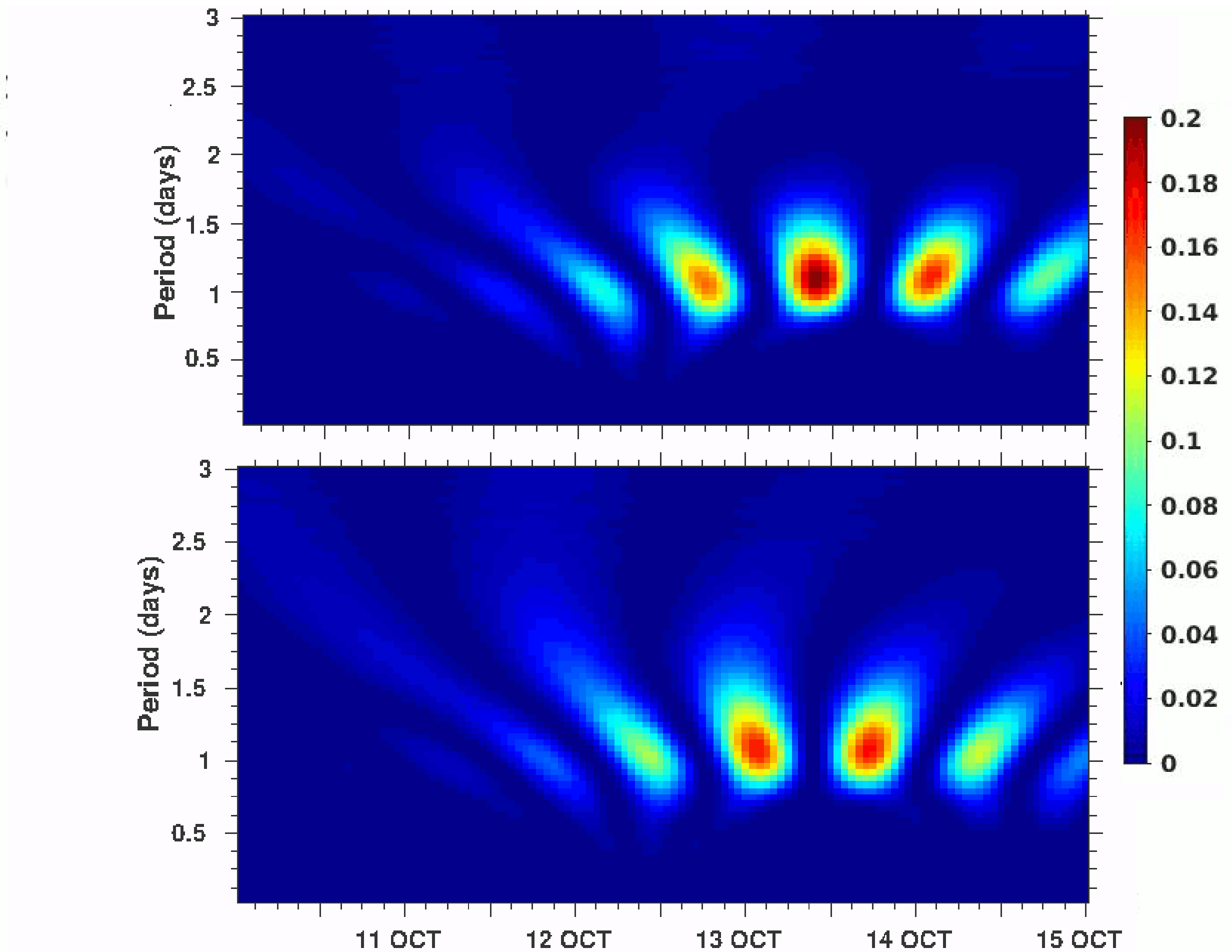

Figure 9:- The scalogram in percentage at 14 m depth by continuous wavelet transform (CWT) method. Wavelet scalogram shown for the zonal baroclinic current (upper panel) and for the meridional baroclinic current (lower panel).

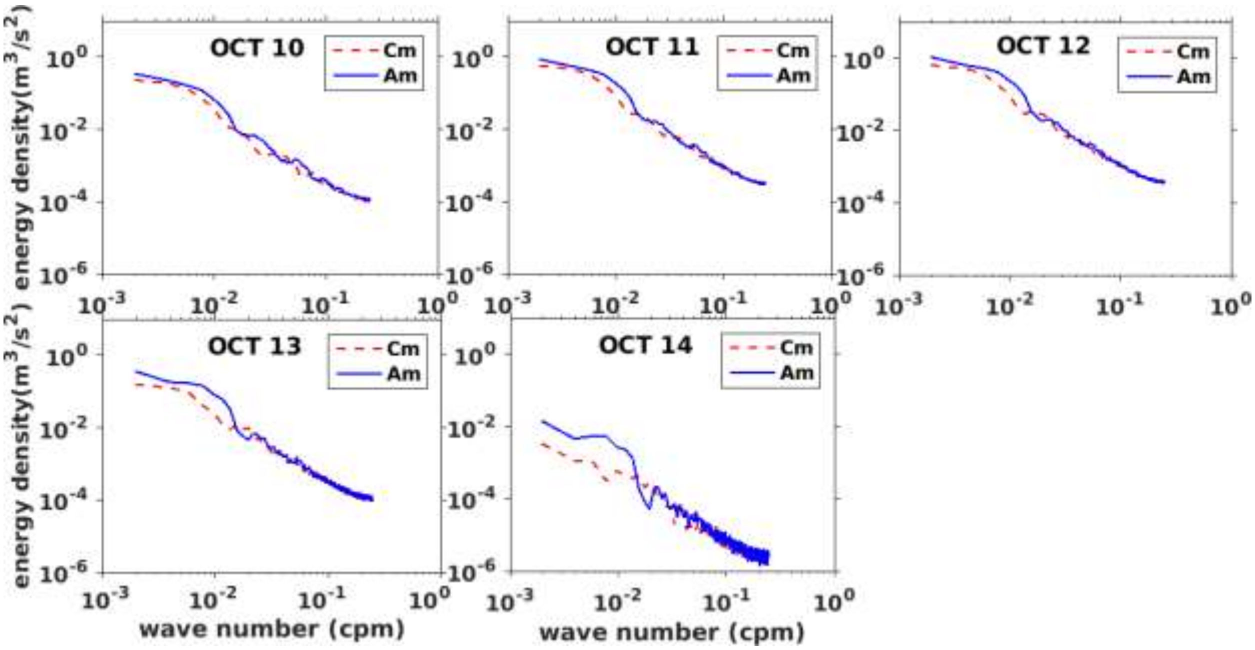

Figure 10:- The daily averaged vertical wave-number rotary spectra of near inertial oscillations. The anticyclonic and cyclonic spectra are represented in blue and dotted red lines respectively.

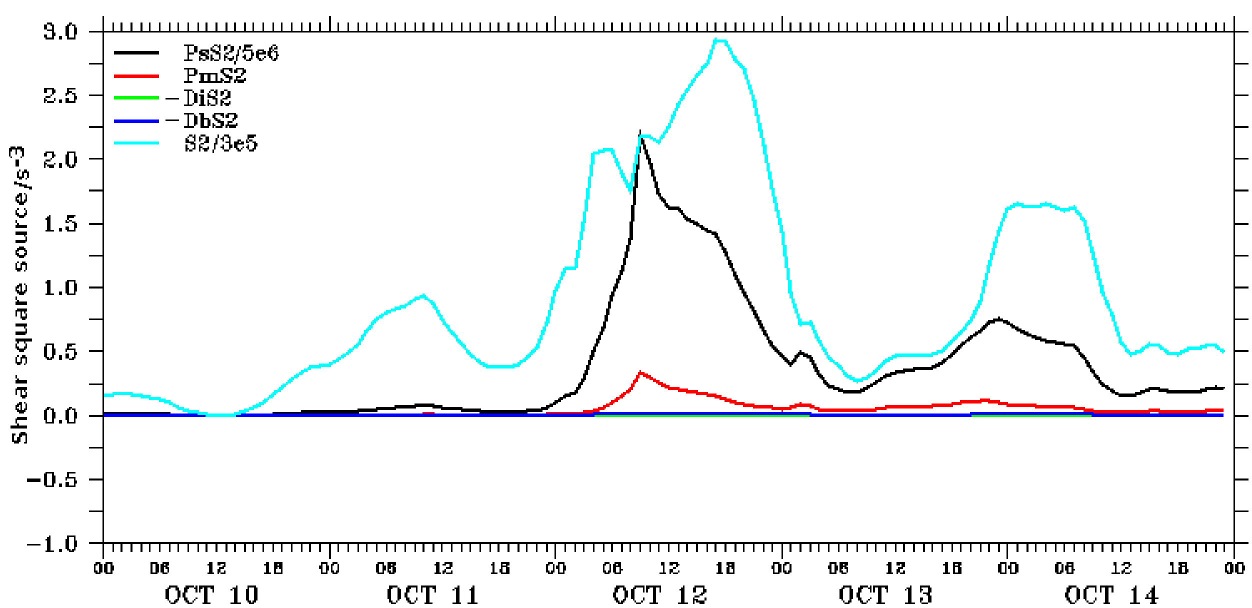

Figure 11:- The model simulated bulk properties at the selected point location. The vertical shear square axis is multiplied with a factor of 10^{-6}. The magnitude of bulk shear squared S^2 (cyan color), surface wind stress P_sS^2 (black color), barotropic effect P_mS^2 (red color), bottom stress $-D_bS^2$ (blue color), interfacial friction $-D_iS^2$ (green color)

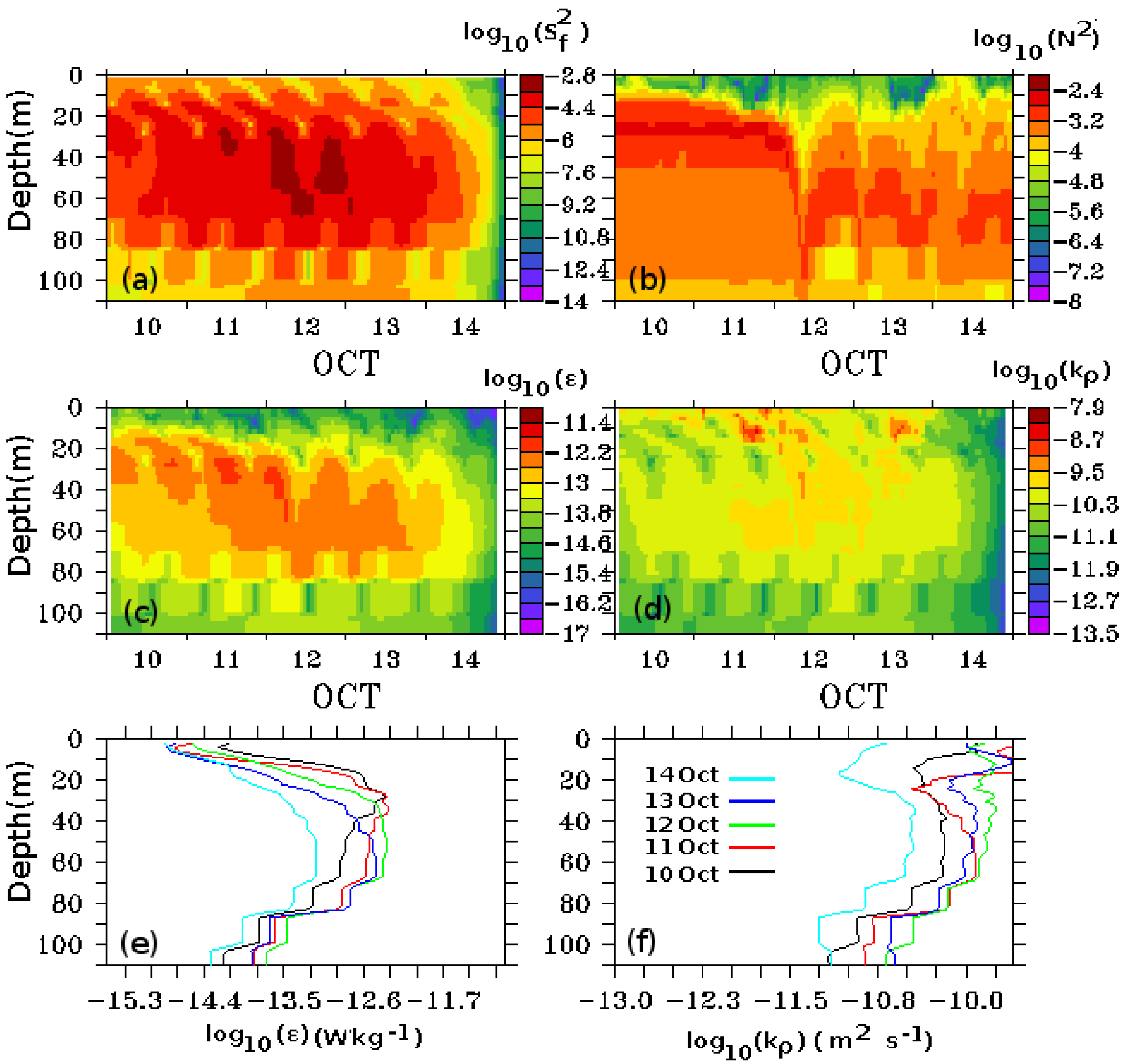

Figure 12:- Profiles of (a) velocity shear $\log_{10}(S^2)$, (b) buoyancy frequency $\log_{10}(N^2)$, (c) turbulent kinetic energy dissipation rate $\log_{10}(\varepsilon)$, (d) turbulent eddy diffusivity $\log_{10}(K\rho)$, (e) and (f) are daily averaged turbulent kinetic energy dissipation rate and turbulent eddy diffusivity respectively